Frontiers of Optoelectronics (2026) 19:11
https://doi.org/10.2738/foe.2026.0011

Frontiers of Optoelectronics

RESEARCH ARTICLE

On-chip vectorial structured light field manipulation by inverse design

Zijia Wang[1*] · Kunhao Lei[1*] · Shenglong Yang[1*] · Mengxue Qi[1] · Jieren Song[1] · Yuting Ye[2] · Hui Ma[1] · Yiting Yun[1] · Qiwei Zhan[1] · Da Li[1] · Shixun Dai[3] · Baile Zhang[4] · Xiaoyong Hu[5] · Lan Li[2] · Erping Li (✉)[1] · Hongtao Lin (✉)[1,6]

Received: 29 November 2025 / Accepted: 29 January 2026

Abstract

Structured light, with its multidimensional control over amplitude, phase, space and frequency, is a key enabler for advanced technologies such as high-capacity communications, quantum information, and super-resolution imaging. Here, we propose a unified inverse-design methodology for arbitrary on-chip vectorial structured-light. Inspired by quantum-state representations, we describe complex vector fields as finite-dimensional vectors in a Hilbert space and introduce a transmission-matrix formalism that links input waveguide modes to target topological edge states. By combining this mapping with adjoint-based topology optimization, we obtain the permittivity distribution within a compact design window that realizes the desired vector transformation while preserving topological transport. We experimentally demonstrate two representative domain-wall configurations on a valley photonic crystal (VPC) platform, termed Type-I and Type-II topological couplers, which efficiently couple the fundamental TE_0 mode into valley pseudospin edge states. Simulations of the ideally designed device show insertion losses of 0.04 dB and 0.09 dB at 1550 nm with 3-dB bandwidths of 132 nm and 65 nm, respectively. Experimentally, the fabricated device, which was designed accounting for fabrication tolerances, maintains a broadband low-loss performance, with measured losses of < 0.6 dB at 1550 nm with 3-dB bandwidth over > 60 nm and $<$ 0.8 dB at 1550 nm with 3-dB bandwidth over 87 nm. Mirror-symmetric designs further validate selective excitation of orthogonal pseudospin states. Our results establish this inverse-design methodology as a powerful tool for strictly controlling on-chip vectorial light, paving the way toward compact, broadband, and multifunctional photonic integrated circuits for optical computing, communications, and beyond.

Keywords Inverse design · On-chip structured light · Valley photonic crystal · Chalcogenide photonics

1 Introduction

Structured light [1,2], with its programmability in multiple degrees of freedom including amplitude, phase, space, frequency and polarization [3–5], represents a frontier field in modern optics. Unlike conventional Gaussian beams or plane waves, structured light offers extended control over spatial and polarization states, such as orbital-angular-momentum (OAM) beams [6], vector beams with spatially varying polarization [7–10], and self-accelerating Airy beams [11]. This diversity of field structures opens new avenues for advanced applications, including high-capacity optical communications [12,13], quantum information processing [13,14], super-resolution imaging [15–17], and optical micromanipulation [18]. However, the generation and manipulation of these fields in free space rely on bulky, alignment-sensitive setups [19], which severely limit their practicality. This fundamental limitation makes the transfer of these capabilities to on-chip integration [20–23] a necessary step toward compact, stable, and scalable optical systems. For this purpose, photonic integrated circuits (PICs) [24–26] offer an ideal platform for bringing on chip structured light into real-world applications [27–29], with the ultimate goal of achieving precise generation and manipulation of complex optical fields.

Valley photonic crystals (VPCs) [30], a key PIC platform, provide an ideal physical platform for on-chip structured-light manipulation [31]. These structures support

*Zijia Wang, Kunhao Lei and Shenglong Yang contributed equally to this work.

Extended author information available on the last page of the article.

pseudospin states characterized by spatially varying field and polarization distributions [32,33]. Their modal field profiles inherently exhibit the essential features of structured light, effectively serving as an on-chip "reservoir" of structured light states. Furthermore, VPCs host two inequivalent valleys ($|K\rangle$ and $|K'\rangle$) as additional degrees of freedom [34] and support topological edge states with distinct chiral responses [35], thereby offering a robust foundation for multidimensional optical control. However, despite this potential, a unified design paradigm for precise on-chip structured-light manipulation within such topological platforms is still lacking.

Inverse design [36,37] offers a new approach. It allows for coordinated control of multidimensional vectorial properties within a compact footprint, while preserving the robust transport characteristics of topological edge states. By directly defining the desired optical functionality and using the adjoint method to optimize in a high-dimensional parameter space [38], inverse design can discover optimal structures that are often inaccessible through traditional empirical approaches. This goal-oriented design paradigm overcomes the limitations of analytic modeling and manual parameter tuning, offering far greater flexibility and performance potential. Adjoint-based inverse optimization has been successfully applied to various photonic devices, such as wavelength demultiplexers [39,40] and logic components [41,42], demonstrating its generality [43,44]. When incorporated into the design of on-chip structured light manipulation, this methodology enables highly flexible, multiparameter control. However, its comprehensive application to vectorial structured light control in topological photonic systems has not yet been systematically explored.

In this work, we propose a quantum-state–inspired [45,46] inverse design methodology that enables arbitrary on-chip manipulation of vectorial structured light on a VPC platform. This methodology models the evolution of the optical field from input to output as a linear transformation in a finite-dimensional Hilbert space. Within this space, a transmission matrix acts as the core operator for the coordinated optimization of spatial, phase, and polarization properties. We designed and realized two compact topological couplers corresponding to distinct domain-wall configurations (Type-I and Type-II). At the 1550 nm telecommunication band, simulations of the ideal design achieved ultralow insertion losses of 0.04 dB and 0.09 dB, with broad 3-dB bandwidths of 132 nm and 65 nm, respectively. Experimentally, the fabricated devices, which were designed accounting for fabrication tolerances, exhibited measured insertion losses below 0.6 dB and 0.8 dB, with 3-dB bandwidths exceeding 60 nm and 80 nm. This study not only verifies the feasibility of achieving precise vector-field control within topological photonic crystals via inverse design but also establishes a unified design paradigm for structured light on-chip, offering a new pathway for developing multifunctional photonic integrated circuits and polarization-multiplexed communication systems.

2 On-chip structure light

The concept of structured light has greatly expanded our ability to manipulate optical fields in multiple dimensions, making its migration from free space to on-chip applications highly attractive. In the context of conventional free-space structured light, engineering amplitude, phase, polarization, and frequency degrees of freedom (DoFs) [3–5] enables the construction of a wide variety of complex light-field distributions (Fig. 1a). Representative free-space structured-light modes shown in Fig. 1 include Gaussian-like OAM modes with zero topological charge $\ell = 0$ (Fig. 1c), as well as OAM beams with a central phase singularity, such as $\ell = 1$ (Fig. 1e), $\ell = 2$ (Fig. 1g), and even higher orders like $\ell = 3$ (Fig. 1i). On chip, the goal is to generate analogous structured textures within guided vectorial fields (see Section S1 in the Supporting Information for definitions). Realizing this capability, however, remains an open problem. Conventional integrated photonic devices predominantly rely on standard transverse electromagnetic modes (TEM, Fig. 1b), which do not explicitly encode rich spatial phase/polarization textures, making it difficult to realize comparable structured-field patterns at the chip scale. It is therefore of significant interest that recent advances in topological photonics provide new physical DoFs and design paradigms for constructing structured light on-chip [24–26], particularly on VPC platforms.

In VPCs, the transverse phase distributions of the interface states often exhibit localized phase-winding patterns. For example, the valley pseudospin mode shown in Fig. 1d displays clear local phase vortices within each unit cell, visually resembling the vortex-like local phase structure found in free-space OAM beams. Similarly, higher-order topological interface states (Fig. 1f) can exhibit double or multiple phase windings at the unit-cell center, with qualitative analogous to free-space OAM modes with $\ell = 2$ (Fig. 1g) or even higher orders (Fig. 1i) of increasing complexity. Meanwhile, the trivial state shown in Fig. 1h presents yet another distinct on-chip field configuration, offering a broader comparison between free-space and chip-based modal structures. Unlike the global topological charge of free-space OAM beams, these localized phase vortices in VPCs originate from the superposition of the valley-degenerate states $|K\rangle$ and $|K'\rangle$, reflecting the valley Chern-number contrast ($\pm$ 1/2) across the interface. Therefore, Fig. 1

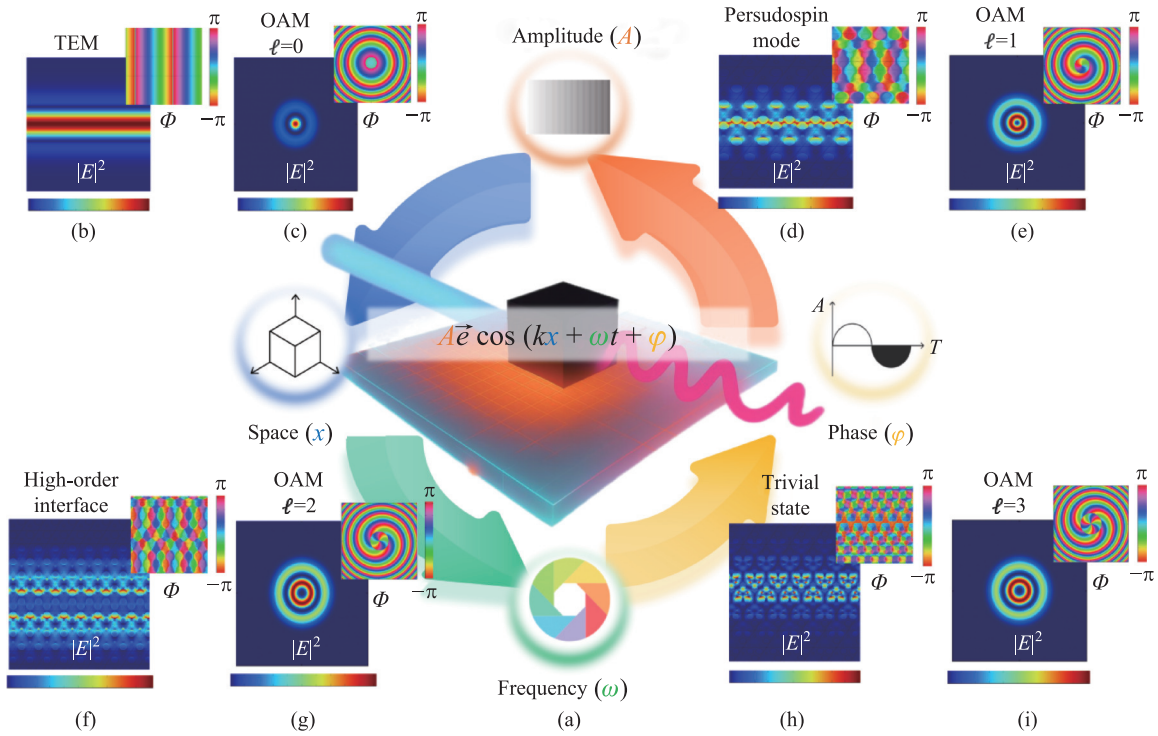

Fig. 1 Inverse design to achieve arbitrary on-chip vectorial structure light conversion. (a) Conceptual illustration of constructing structured light using four fundamental degrees of freedom (DoFs): spatial distribution, amplitude, phase, and frequency. These DoFs enable the generation of diverse structured-light patterns in both free space and integrated photonic platforms. **Free-space structured light (c, e, g, i)**. (c) OAM beam with $\ell = 0$, showing a Gaussian-like intensity distribution and uniform phase. (e) OAM beam with $\ell = 1$, exhibiting a single-charge helical phase vortex and doughnut intensity. (g) OAM beam with $\ell = 2$, displaying a double-charge phase winding consistent with higher-order vortex beams. (i) OAM beam with $\ell = 3$, showing a triple-charge spiral phase and expanded annular intensity. **On-chip structured light (b, d, f, h)**. (b) Transverse electromagnetic mode (TEM) supported by a waveguide structure, representing a basic on-chip spatial mode without topological charge. (d) Pseudospin mode in a valley photonic crystal (VPC), formed by superposition of degenerate valley states and characterized by staggered phase textures with local vortices. (f) High-order photonic-crystal interface state, featuring multiple phase lobes shaped by the periodic refractive-index modulation. (h) Trivial photonic-crystal mode, showing periodic phase and intensity modulation but lacking topological protection.

as a whole illustrates the correspondence between free-space structured-light modes (Fig. 1c, e, g, i) and on-chip topological structured-light modes (Fig. 1b, d, f, h) in terms of phase, amplitude, and spatial patterns, highlighting that topological photonic platforms can naturally support high-dimensional vectorial light fields analogous to structured light, thus providing a physical foundation for realizing structured light on-chip. (See Section S1 in the Supporting Information for a rigorous discussion).

Looking beyond the devices demonstrated in this work, the inverse-design method introduced here is inherently extensible and offers a unified pathway toward multidimensional structured-light manipulation on integrated photonic platforms. While our study focuses on vectorial transformations between conventional strip-waveguide modes and valley pseudospin states, the same transmission-matrix formalism can be generalized to accommodate additional optical degrees of freedom. In the phase domain, the method may enable broadband, topology-compatible phase modulation elements, forming the basis for reconfigurable interferometric units or phase-controlled logic within topological photonic circuits. In the wavelength domain, extending the mapping matrix toward joint space–wavelength–valley control could support novel wavelength-division functionalities and selective spectral routing, which are essential for scaling future quantum and classical communication architectures. Furthermore, in the spatial domain, the inverse-design strategy may facilitate direct conversion between free-space structured beams and topological edge states, establishing on-chip interfaces capable of bridging free-space channels, optical fibers, and topological photonic crystals. More broadly, since the framework can naturally evolve from a matrix representation into a high-dimensional tensor formulation, it may eventually enable simultaneous control over phase, wavelength, polarization, orbital angular momentum, and temporal properties within a single design paradigm. These prospects highlight the versatility and scalability of inverse-designed topological photonics and

point toward a promising route for realizing compact, broadband, and multifunctional integrated platforms for advanced optical signal processing and quantum information technologies.

3 Structure light manipulation by inverse design

To achieve arbitrary on-chip manipulation of vectorial structured light within a VPC platform, we employ a quantum-state–inspired representation to guide the inverse design framework centered on the transmission matrix, as illustrated in Fig. 2. It provides a compact Hilbert-space notation, which arises as the vector space spanned by orthogonal spatial and polarization modes naturally and provides a rigorous framework for describing field superposition and linear optical transformations (see Section S2 in the Supporting Information for a detailed discussion). We could represent any on-chip vectorial structured light field as a quantum-state superposition of basis vectors [46]:

$$|E\rangle = \sum_{i=1}^{N} \sum_{j\in\{x,y,z\}} C_{ij}|r_i\rangle \otimes \left|p_j\right\rangle.$$

Here, $|r_i\rangle$ denotes the basis state associated with the i-th spatial sampling point on the observation plane, N is the total number of spatial sampling points, and $\left|p_j\right\rangle$denotes the orthonormal polarization basis state corresponding to the Cartesian unit vector $\hat{e}_j$. The complex coefficient C_{ij} corresponds to the complex electric-field amplitude of the j-th polarization component evaluated at the spatial location r_i, thereby encoding the amplitude and phase information of the structured light field. Directly operating in a continuous, infinite-dimensional space is neither necessary nor efficient for numerical implementation. Therefore, we sample the vectorial fields on selected transverse planes, restricting the spatial and polarization degrees of freedom to a finite set. Consequently, the input and output fields are represented as finite-dimensional complex matrices:

$$E_{\text{in}} \in C^{N_{\text{in}}\times d}, E_{\text{out}} \in C^{N_{\text{out}}\times d},$$

where $N_{\text{in}}/N_{\text{out}}$ denote the number of sampling points or modes, d denotes the dimensionality of the polarization subspace, and C denotes the complex number field. When the spatial sampling grid is sufficiently dense and the discretization satisfies the constraints of Maxwell's equations, this representation is information-equivalent to the original continuous vector field. It thus serves as the computational workspace for subsequent modeling and optimization, as illustrated in Fig. 2a (for more information regarding the selection criteria for the discretized-observation plane and clarifications, see Section S4 in the Supporting Information). Under this representation, the device functionality can be abstracted as a linear transformation from E_{in} to E_{out}:

$$E_{\text{out}} = T \cdot E_{\text{in}},$$

where T is the transmission matrix, which characterizes how the input spatial-polarization states are transformed into the target structured-light states within the chosen finite-dimensional basis. Physically, T encodes the scattering and propagation behavior of electromagnetic waves under the given dielectric distribution. For the operator-level derivation relating the continuous Maxwell operator to the finite-dimensional transmission matrix (via projection/synthesis operators), see Section S3 in the Supporting Information.

In this work, we first specify the desired target field E_{out}, such as achieving efficient, phase-preserving, or polarization-selective transformation from the single-mode waveguide TE_0 mode to a specific topological pseudospin edge state. Subsequently, by numerically solving Maxwell's equations, we establish the mapping from the dielectric permittivity distribution $\varepsilon(r)$ inside the device to the transmission matrix $T(\varepsilon)$ evaluated on the discretized observation plane. Figure 2a conceptually illustrates the relationship among the input optical field, the transmission matrix, and the target vectorial structured-light state. It depicts how, within the chosen finite-dimensional basis, the input spatial–polarization states are mapped to the desired output state. The complete three-dimensional evolution of the optical field can be reconstructed by solving Maxwell's equations numerically on a discretized grid, ensuring the accuracy of this mapping within its finite-dimensional representation.

Using the inverse-design optimization algorithm, we design a nonuniform dielectric permittivity distribution within a predefined compact region to realize the desired transmission matrix. The overall design workflow is illustrated in Fig. 2b. After defining the target mapping and monitors, the design is parameterized by a pixelated density field within the optimization window. In each iteration, a forward simulation evaluates the figure of merit (FOM) associated with the desired transmission-matrix mapping, and an adjoint simulation provides the gradient with respect to the design variables. A gradient-based optimizer then updates the design field. To obtain physically realizable layouts, the updated design is processed by spatial filtering (e.g., top-hat convolution) and a projection step (e.g., a Heaviside-type mapping), which progressively drives the permittivity distribution toward a near-binary two-material pattern. The projection strength is increased through a continuation scheme until the design becomes sufficiently bi-

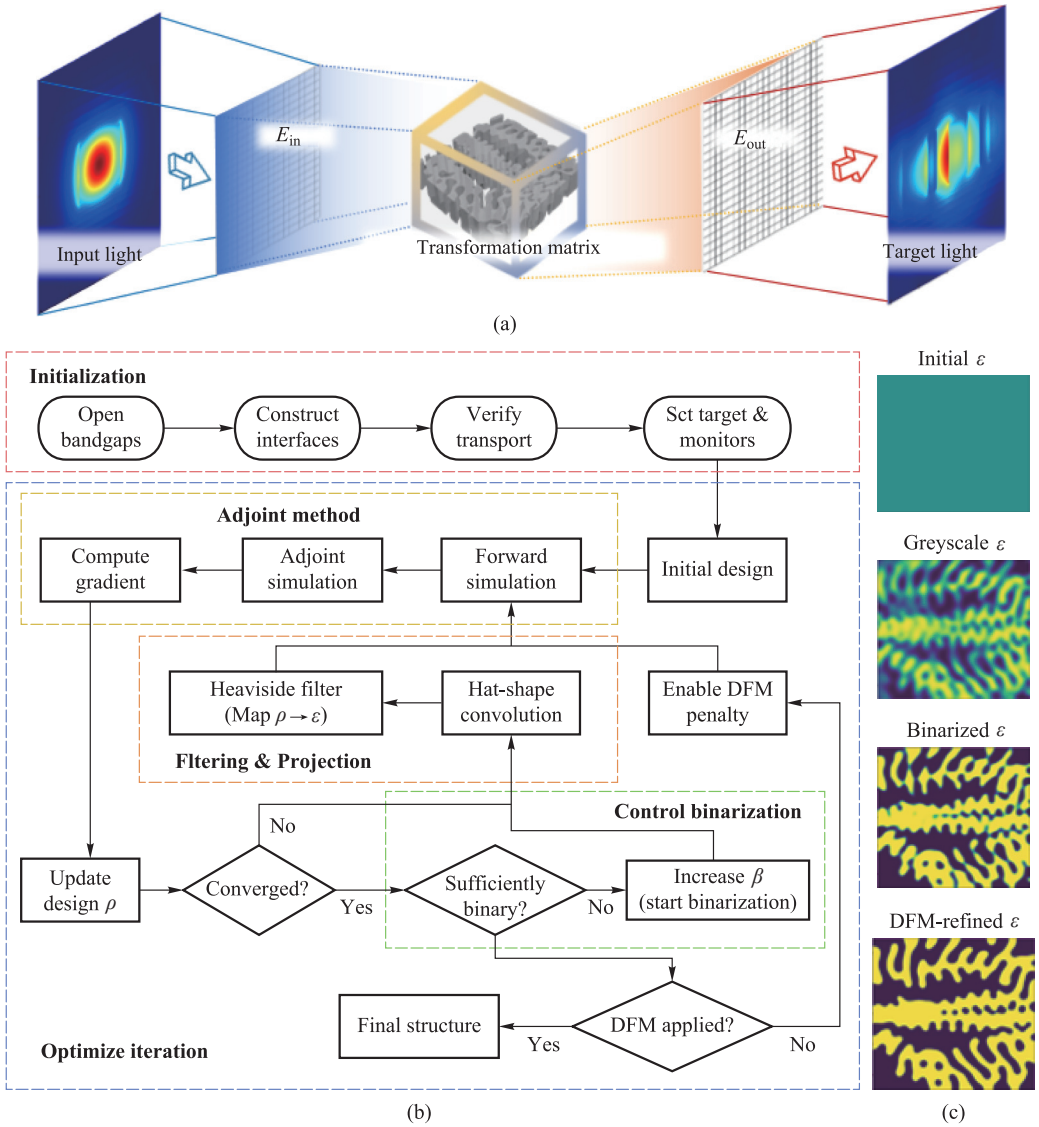

Fig. 2 Unified transformation-matrix-based framework for on-chip vectorial structured light. (a) The input and target vectorial fields are discretized into finite-dimensional matrices, and their relation is described by a transmission matrix T mapping E_{in} to E_{out}. (b) Inverse-design workflow under the transmission-matrix constraint. (c) Evolution of the permittivity distribution during optimization from an initial continuous parameterization to a near-binary and finally manufacturable layout. **Initial** ε: user-defined starting distribution within the design domain. **Greyscale** ε: A smoothed mapping converts the continuous design variables into a graded permittivity distribution between the two materials; top-hat convolution is applied to suppress unstable fine features. **Binarized** ε: The material distribution is parameterized by a density field ($\rho \in [0,1]$). A spatial filter (top-hat convolution) is applied to ρ for regularization. The filtered density is then projected to a physical permittivity via a smooth Heaviside function (with a low β value), resulting in a continuous ε distribution between ε_{min} and ε_{max}. **DFM-refined** ε: A minimum-feature-size constraint is enforced by adding a penalty term to the FOM, improving fabrication robustness.

narized. To improve the manufacturability of the optimized designs, we incorporate a design-for-manufacturing (DFM) stage into the topology-optimization workflow. By introducing a minimum-feature-size penalty term, this stage suppresses ultra-fine structures that are sensitive to fabrication errors, thereby enhancing process robustness, albeit at the cost of some ideal simulated performance. Representative permittivity patterns in different stages are shown in Fig. 2c. Further workflow details are provided in Section S5 of the Supporting Information.

Traditional optical-field control approaches often rely on analytical formulations, which become cumbersome for complex vectorial fields—especially on-chip structured light in VPCs. In contrast, our framework provides a unified, implementation-friendly route by constructing a transmission matrix that maps between input and target vectori-

al field states within a chosen finite-dimensional basis, while being physically realized by a compact dielectric structure governed by Maxwell's equations. Importantly, this transmission-matrix–based inverse-design paradigm is not limited to the pseudospin edge states demonstrated here: once the desired target field is specified on the observation plane(s), the same workflow can be directly extended to synthesize and manipulate other representative vectorial structured-light states (e.g., cylindrical vector beams [8], etc.) on chip, by appropriately defining the target amplitude–phase–polarization distribution and the corresponding figure of merit.

4 Inverse designed coupler for topological photonics

The efficient coupling between standard single-mode strip waveguides and topological photonic crystals is fundamentally limited by modal field mismatch. Here, we systematically overcome this limitation using our inverse-design framework, designing two compact couplers for distinct valley-topological domain-wall configurations.

The first configuration, referred to as the Type-I domain wall, consists of two interleaved honeycomb valley photonic crystal lattices (VPC1 and VPC2), as shown in Fig. 3a, forming a complete valley photonic crystal structure illustrated in Fig. 3b and 3c. By breaking spatial inversion symmetry via a structure with $a = 480$ nm, $R = 223$ nm, and $r = 78$ nm, a photonic bandgap is opened in the 1460–1630 nm wavelength range (Fig. 3d). Due to the valley Hall effect, light propagates along the interface between the two oppositely polarized VPC regions in the form of pseudospin modes. Previous studies have attempted coupling through line-defect waveguides, multimode waveguides, or asymmetric junctions; however, these approaches often suffer from high insertion loss (IL), large footprint, or the inability to achieve single-mode coupling.

Using the aforementioned inverse-design approach, we designed a compact 5 μm × 5 μm structure, which is referred to as the Type-I coupler, that satisfies the transmission-matrix mapping between the TE_0 mode and the valley pseudospin field. The optimization objective was defined over the target wavelength band of 1540−1560 nm and the resulting ideal design is shown in Fig. 3e. The device connects a single-mode strip waveguide (500 nm × 200 nm) to the VPC, and its optical-intensity distribution was simulated at a wavelength of 1550 nm. Under ideal fabrication conditions, the Type-I coupler achieves an insertion loss of only 0.04 dB at 1550 nm (Fig. 3g, red dashed line, simulated result) and exhibits a 3-dB bandwidth of 132 nm (1484−1616 nm), enabling efficient conversion of the wavevector from the TE_0 mode into the pseudospin mode within the VPC. Figure 3g and 3i comprehensively demonstrate the superiority of our design. At the wavelength of 1550 nm, optical energy injected from the single-mode waveguide into the topological coupler enters the valley photonic crystal with near-zero reflection, and then continues seamlessly into the output waveguide (Fig. 3i, left).

For comparison, when the VPC is directly connected to the single-mode waveguide (Fig. 3i, center), the field mismatch causes significant insertion loss (IL = 2.54 dB @ 1550 nm, green dashed line in Fig. 3g) and oscillations along the transmission path. Simulated power-flow distributions clearly show standing-wave patterns both inside the waveguide and within the photonic crystal, indicating strong back-reflection. It is also noteworthy that the two pseudospin modes possess spatial chiral symmetry. Aligning the Type-I coupler in a mirror-symmetric configuration enables excitation of the orthogonal pseudospin mode. As shown in Fig. 3i (right), the injected pseudospin light corresponds to the opposite local handedness (RCP instead of LCP) due to selective excitation of the opposite pseudospin branch. Under ideal fabrication conditions, the coupler yields a peak extinction ratio (ER) of 11.79 dB at 1550 nm (the difference between the insertion loss of the red curve and that of the blue dashed curve in Fig. 3g). This behavior arises because the two pseudospin modes in the VPC are orthogonal and counter-propagating, causing optical energy to remain largely confined within the input waveguide and suppressing transmission into the photonic-crystal region when the opposite pseudospin is excited.

In addition to the ideal design in Fig. 3e, we carried out a fabrication-aware re-optimization to obtain the fabrication-aware design shown in Fig. 3f. Fabrication tolerance is incorporated at the optimization level by imposing manufacturability constraints via spatial filtering and a minimum-feature-size control. Concretely, a larger filtering strength is applied and a minimum-feature-size penalty is enabled to eliminate ultra-fine features (e.g., small islands, sharp corners, and narrow bridges) that are highly sensitive to lithography/etching variations. As a result, the fabrication-aware design is obtained by re-optimizing the structure under stricter constraints rather than by simply correcting or smoothing the ideal design. Since the feasible design space is reduced by these constraints, the fabrication-aware design can exhibit a different field pattern and a slightly degraded ideal simulated performance, but it is expected to be more robust and closer to experimental behavior under the available fabrication process. Taking into account the constraints of the fabrication platform, we fabricated the fabricated device based on this fabrication-aware design, and the measured results are shown in Fig. 3h. The measured

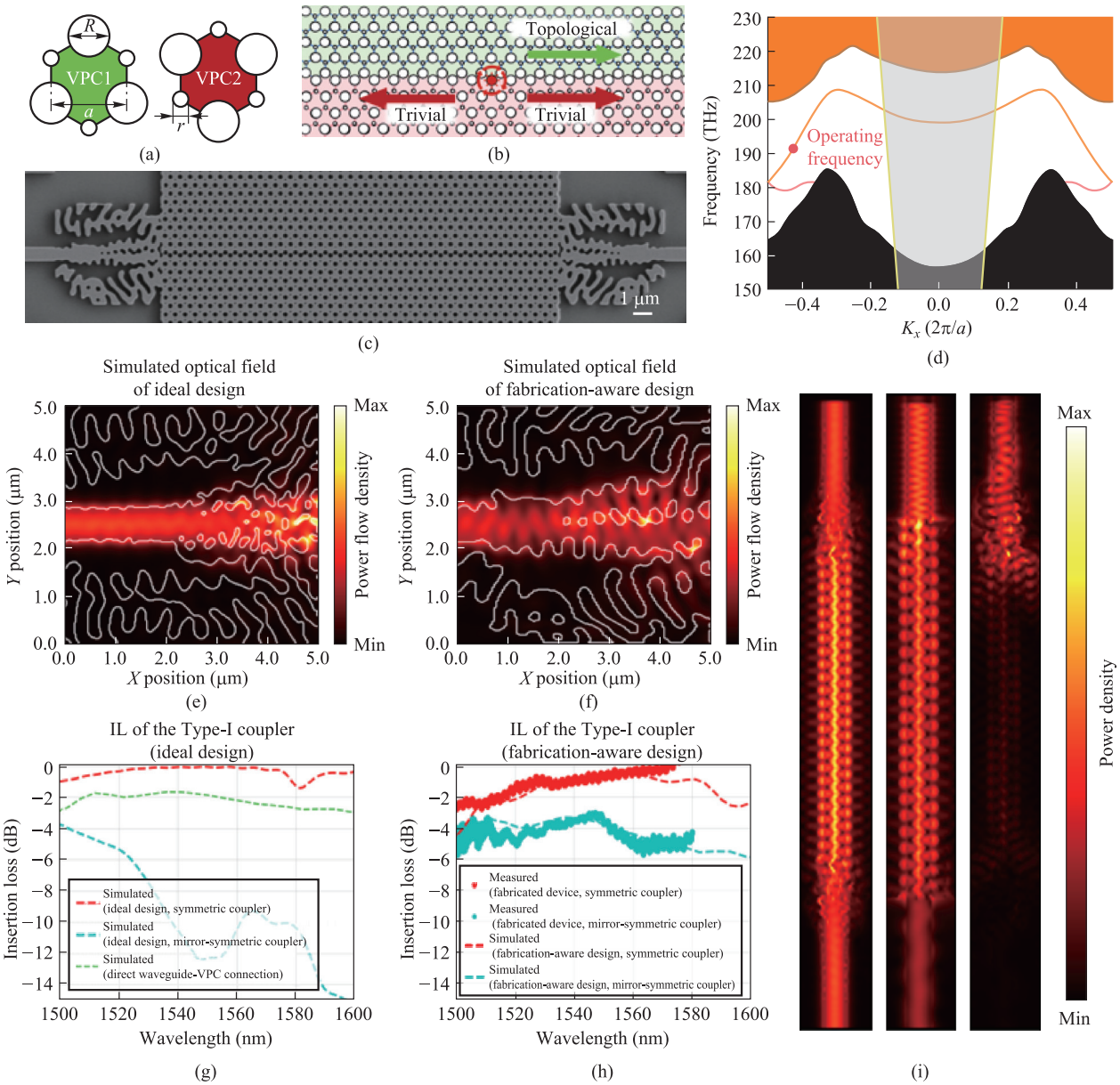

Fig. 3 Inverse-designed Type-I coupler enabling efficient coupling between a single-mode strip waveguide and a valley photonic crystal. (a) Schematic of two honeycomb valley photonic crystal unit cells (VPC1/VPC2). (b) Schematic of the topological/trivial regions and their interface formed by VPC1/VPC2. (c) SEM image of the fabricated device with an inverse-designed coupling region of approximately 5 μm × 5 μm. (d) Illustration of the bandgap and operating frequency range opened by breaking spatial inversion symmetry. (e) Optical intensity distribution at 1550 nm for the ideal design, showing efficient conversion from the TE_0 mode to the valley pseudospin mode. (f) Optical intensity distribution of the fabrication-aware design. (g) Simulated insertion loss spectra of the Type-I couplers based on ideal design, direct connection, and its mirror-symmetric coupler. (h) Simulated insertion loss spectra of fabrication-aware design (based on the fabrication-aware design) and measured insertion loss spectra of the corresponding fabrication-aware designs for the symmetric and mirror-symmetric couplers. (i) Energy flow distributions for three structures: the inverse-designed coupler achieves near-zero-reflection coupling, the direct connection exhibits strong reflection and standing waves, and the mirror-symmetric coupler selectively excites the opposite-chirality pseudospin mode.

results, indicated by the red dotted line, show an insertion loss of 0.58 dB at 1550 nm, with a 3-dB bandwidth exceeding 60 nm (ranging from 1526 nm to 1586 nm).

The Type-II domain wall is obtained by symmetrically transforming the VPC configuration shown in Fig. 3a, resulting in two new VPCs illustrated in Fig. 4a. When arranged together, they form a distinct topological boundary state, as shown in Fig. 4b, the Type-II domain wall opens a photonic bandgap spanning 1440–1620 nm (Fig. 4d). Using the same inverse-design procedure, we constructed the

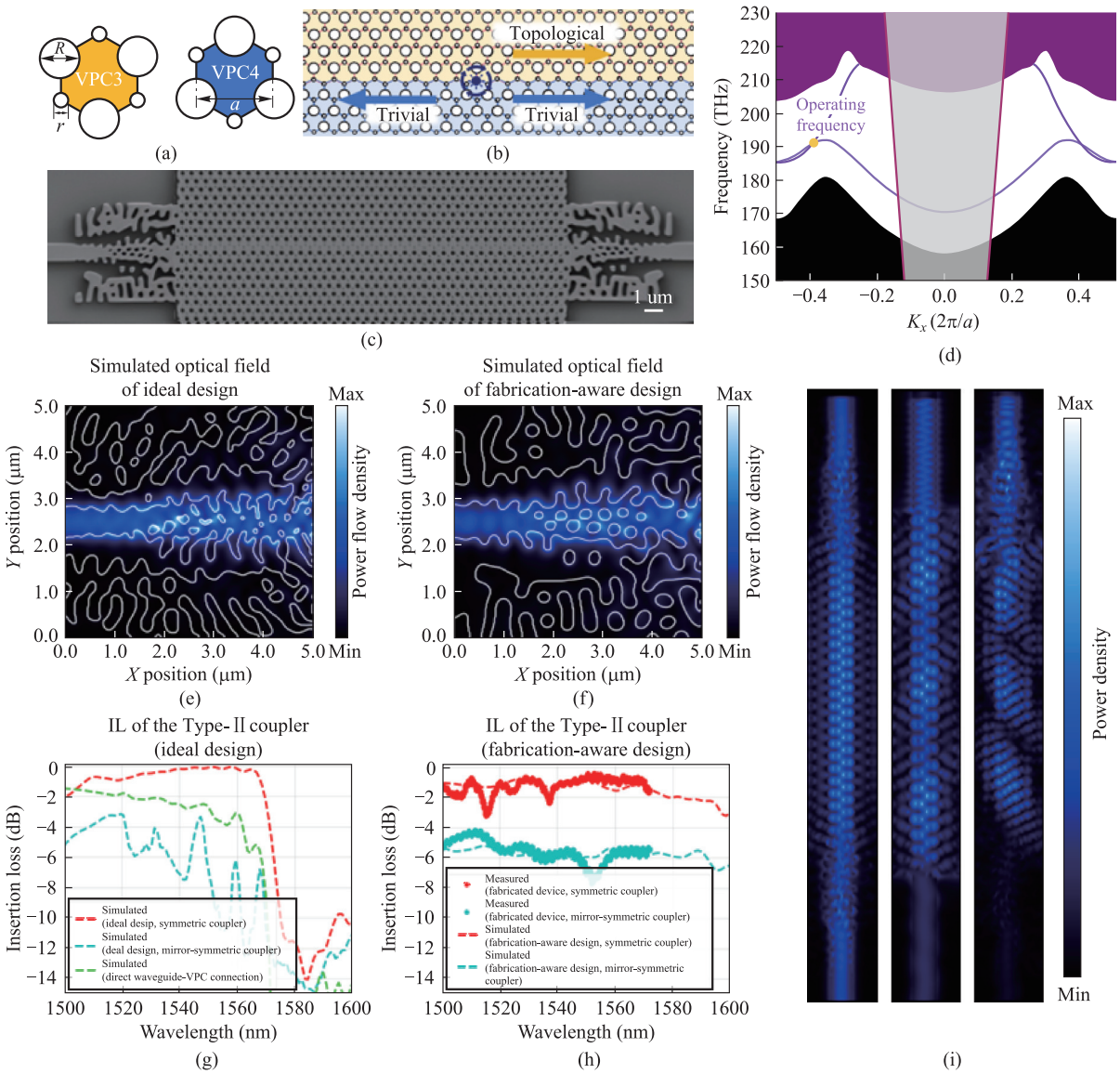

Fig. 4 Inverse-designed Type-II coupler enabling efficient coupling between a single-mode strip waveguide and a valley photonic crystal. (a) Schematic of two honeycomb valley photonic crystal unit cells (VPC3/VPC4). (b) Schematic of the topological/trivial regions and their interface formed by VPC3/VPC4. (c) SEM image of the fabricated device with an inverse-designed coupling region of approximately 5 μm × 5 μm. (d) Illustration of the bandgap and operating frequency range opened by breaking spatial inversion symmetry. (e) Optical intensity distribution at 1550 nm for the ideally designed device, showing efficient conversion from the TE0 mode to the valley pseudospin mode. (f) Optical intensity distribution of the fabrication-aware design. (g) Simulated insertion loss spectra of the Type-II couplers based on ideal design, direct connection, and its mirror-symmetric coupler. (h) Simulated insertion loss spectra of fabrication-aware design (based on the fabrication-aware design) and measured insertion loss spectra of the corresponding fabrication-aware designs for the symmetric and mirror-symmetric couplers. (i) Energy flow distributions for three structures: the inverse-designed coupler achieves near-zero-reflection coupling, the direct connection exhibits strong reflection and standing waves, and the mirror-symmetric coupler selectively excites the opposite-chirality pseudospin mode.

Type-II coupler (Fig. 4c) to verify that the proposed framework can adaptively optimize different domain-wall configurations with the optimization objective defined over the target wavelength band of 1540–1560 nm. Under ideal fabrication conditions, the ideal design achieved an insertion loss of 0.09 dB at 1550 nm (Fig. 4g, red dashed line, simulated result) and a 3 dB bandwidth of 65 nm (1504–1569 nm), realizing efficient wavevector conversion from the TE_0 mode to the pseudospin mode in the VPC. Figure 4i presents the optical-intensity distributions resulting from excitation through the ideal design of Type-II coupler, a direct connection, and its mirror-symmetric counterpart. Similar to the Type-I coupler, the Type-II coupler enables near-zero-loss mode conversion. In contrast,

direct coupling between the single-mode waveguide and VPC (Fig. 4i, middle) causes significant field mismatch, resulting in an insertion loss of 3.17 dB at 1550 nm (Fig. 4g, green dashed line, simulation). With the mirror-symmetric configuration, the device exhibits a peak extinction ratio (ER) of 10.55 dB at 1554 nm, defined as the transmission contrast between the two opposite pseudospin excitations (Fig. 4g, simulation). Finally, the fabricated device based on the fabrication-aware design was fabricated on the GSSe chalcogenide glass platform, as shown in Fig. 4c. The fabricated device (Fig. 4f) exhibits an insertion loss of 0.77 dB at 1550 nm and a 3 dB bandwidth of 87 nm (1486−1573 nm), as indicated by the red dotted line in Fig. 4h, in good agreement with simulation results of the fabrication-aware design.

5 Conclusion

In conclusion, we have proposed and experimentally demonstrated an inverse-design-based framework for on-chip vectorial structured-light manipulation, achieving efficient control of complex optical fields on a VPC platform, achieving efficient and low-loss coupling from conventional waveguide modes to topological pseudospin states. By introducing a quantum-inspired mapping matrix, the optical-field conversion problem in an infinite-dimensional Hilbert space is transformed into a finite-dimensional matrix optimization, enabling precise control of complex vector fields. Simulations of the ideally designed device show insertion losses of 0.04 dB and 0.09 dB at 1550 nm with 3-dB bandwidths of 132 nm and 65 nm, respectively. Measurements of the fabricated device, which was designed to account for fabrication tolerances, confirm a broadband low-loss performance, with losses below 0.6 dB at 1550 nm with 3-dB bandwidth over > 60 nm and below 0.8 dB at 1550 nm with 3-dB bandwidth over 87 nm. These results validate the effectiveness and practicality of inverse design for topological photonics, advancing the field from passive transport toward active control, and paving the way for high-performance, multifunctional integrated photonic circuits such as optical neural networks and quantum photonic chips.

Supplementary Information The online version contains supplementary material available at https://doi.org/10.2738/foe.2026.0011.

Acknowledgements This work was supported by the National Key Research and Development Program of China (No. 2024YFB2808700), "Pioneer" R&D Program of Zhejiang (No. 2025C01002), and the Key Project of Westlake Institute for Optoelectronics (No. 2024GD002). The authors would like to acknowledge the fabrication support from the ZJU Nano-Fabrication Center at Zhejiang University, the Westlake Center for Micro/Nano Fabrication and Instrumentation at Westlake University, and the Nano-Fabrication Center at Zhejiang Laboratory.

Author contributions H.L. conceived the idea. Z.W. wrote the code and designed the device. S.Y. performed the topological simulations. Z.W., K.L., M.Q., Y.Y., H.M. participated in the fabrication process. Z.W. carried out the device testing. J.S. provided support for the free-space optical simulations. Q.Z., D.L., S.D., H.L., B.Z., X.H., L.L, and E.L. supervised the research. All the authors contributed to the technical discussions and writing of the paper.

Availability of data and materials The data that support the findings of this study are available from the corresponding author, upon reasonable request.

Declarations

Competing interests The authors declare that they have no competing financial interests.

Appendixes

A.1 Methods

1) Fabrication [47]
The chalcogenide glass (ChG) film was composed of $Ge_{28}Sb_{12}Se_{60}$. The thin films (500 nm thickness) were deposited on top of a standard silicon wafer with 2 μm thick silicon oxide by thermal evaporation. The film was then spin-coated by the positive-tone e-beam resist (ARP 6200.13). The photonic crystals and the inverse design structure were patterned by using electron beam lithography (Raith VOYAGER). The ChG of the electron beam exposed area was then etched by inductively coupled plasma etching (Oxford Plasmapro100 Cobra 180) and the patterns were finally transferred to the film by the removal of the e-beam resist.
2) Optical measurements [48]
The C band test system for the measurement was mainly composed of a broadband tuning laser (Santec TSL-570), a vertical fiber coupling platform, and a photodetector (MPM-210/210-H). The polarization direction of the light

was controlled using a manual polarization controller. The transmission spectrum was measured by scanning the wavelength of the laser, and the output signal power was detected by the photodetector.

A.2 Inverse design method

Except for the proposed initialization strategy, the inverse-design procedure follows the standard adjoint-based topology optimization implemented in the Lumerical lumopt framework. In each iteration, a forward simulation evaluates the objective function F defined by the target mapping, and an adjoint simulation provides the gradient $\partial F/\partial \epsilon(r)$. The design is then updated using the L-BFGS optimizer. To enforce manufacturable features and promote a near-binary permittivity distribution, spatial filtering and a Heaviside projection are applied, with the projection sharpness parameter β following the default β-continuation scheme in lumopt. The optimization terminates when the objective change satisfies the convergence criterion $|\Delta F| < 0.001$. After convergence, an optional binarization/DFM step is performed to obtain the final fabricable structure.

For the ideal design we used filter_R = 60 nm and min_feature_size = 60 nm, whereas for the fabrication-aware design we used filter_R = 180 nm and min_feature_size = 90 nm.

References

1. Forbes, A., De Oliveira, M., Dennis, M.R.: Structured light. Nat. Photonics **15**(4), 253–262 (2021)
2. Nape, I., Singh, K., Klug, A., Buono, W., Rosales-Guzman, C., McWilliam, A., Franke-Arnold, S., Kritzinger, A., Forbes, P., Dudley, A., Forbes, A.: Revealing the invariance of vectorial structured light in complex media. Nat. Photonics **16**(7), 538–546 (2022)
3. Zang, W., Yuan, Q., Chen, R., Li, L., Li, T., Zou, X., Zheng, G., Chen, Z., Wang, S., Wang, Z., Zhu, S.: Chromatic dispersion manipulation based on metalenses. Adv. Mater **32**(27), e1904935 (2020)
4. Yu, N., Capasso, F.: Flat optics with designer metasurfaces. Nat. Mater **13**(2), 139–150 (2014)
5. Zou, X.J., Zheng, G.G., Yuan, Q., Zang, W., Chen, R., Li, T., Li, L., Wang, S., Wang, Z., Zhu, S.: Imaging based on metalenses. PhotoniX **1**(1), 2 (2020)
6. Berry, M.: Making waves in physics. Nature **403**(6765), 21 (2000)
7. Bauer, T., Banzer, P., Karimi, E., Orlov, S., Rubano, A., Marrucci, L., Santamato, E., Boyd, R.W., Leuchs, G.: Observation of optical polarization Möbius strips. Science **347**(6225), 964–966 (2015)
8. Mao, D., Zheng, Y., Zeng, C., Lu, H., Zhao, J.: Generation of polarization and phase singular beams in fibers and fiber lasers. Adv. Photon **3**(1), 014002 (2021)
9. Liu, M., Huo, P., Zhu, W., Zhang, C., Zhang, S., Song, M., Zhang, S., Zhou, Q., Chen, L., Lezec, H.J., Agrawal, A., Lu, Y., Xu, T.: Broadband generation of perfect Poincaré beams via dielectric spin-multiplexed metasurface. Nat. Commun **12**(1), 2230 (2021)
10. Ndagano, B., Nape, I., Cox, M.A., Rosales-Guzman, C., Forbes, A.: Creation and detection of vector vortex modes for classical and quantum communication. J. Lightwave Technol **36**(2), 292–301 (2018)
11. Efremidis, N.K., Chen, Z., Segev, M., Christodoulides, D.N.: Airy beams and accelerating waves: an overview of recent advances. Optica **6**(5), 686 (2019)
12. Wang, J., Yang, J.Y., Fazal, I.M., Ahmed, N., Yan, Y., Huang, H., Ren, Y., Yue, Y., Dolinar, S., Tur, M., Willner, A.E.: Terabit free-space data transmission employing orbital angular momentum multiplexing. Nat. Photonics **6**(7), 488–496 (2012)
13. Willner, A.E., Huang, H., Yan, Y., Ren, Y., Ahmed, N., Xie, G., Bao, C., Li, L., Cao, Y., Zhao, Z., Wang, J., Lavery, M.P.J., Tur, M., Ramachandran, S., Molisch, A.F., Ashrafi, N., Ashrafi, S.: Optical communications using orbital angular momentum beams. Adv. Opt. Photonics **7**(1), 66 (2015)
14. Arrazola, J.M., Bergholm, V., Brádler, K., Bromley, T.R., Collins, M.J., Dhand, I., Fumagalli, A., Gerrits, T., Goussev, A., Helt, L.G., Hundal, J., Isacsson, T., Israel, R.B., Izaac, J., Jahangiri, S., Janik, R., Killoran, N., Kumar, S.P., Lavoie, J., Lita, A.E., Mahler, D.H., Menotti, M., Morrison, B., Nam, S.W., Neuhaus, L., Qi, H.Y., Quesada, N., Repingon, A., Sabapathy, K.K., Schuld, M., Su, D., Swinarton, J., Száva, A., Tan, K., Tan, P., Vaidya, V.D., Vernon, Z., Zabaneh, Z., Zhang, Y.: Quantum circuits with many photons on a programmable nanophotonic chip. Nature **591**(7848), 54–60 (2021)
15. Devlin, R.C., Ambrosio, A., Rubin, N.A., Mueller, J.P.B., Capasso, F.: Arbitrary spin-to-orbital angular momentum conversion of light. Science **358**(6365), 896–901 (2017)
16. Curd, A., Cleasby, A., Makowska, K., York, A., Shroff, H., Peckham, M.: Construction of an instant structured illumination microscope. Methods **88**, 37–47 (2015)
17. York, A.G., Chandris, P., Nogare, D.D., Head, J., Wawrzusin, P., Fischer, R.S., Chitnis, A., Shroff, H.: Instant super-resolution imaging in live cells and embryos via analog image processing. Nat. Methods **10**(11), 1122–1126 (2013)
18. Yang, Y., Ren, Y.X., Chen, M., Arita, Y., Rosales-Guzmán, C.: Optical trapping with structured light: a review. Adv. Photon **3**(3), 034001 (2021)
19. Rubinsztein-Dunlop, H., Forbes, A., Berry, M.V., Dennis, M.R., Andrews, D.L., Mansuripur, M., Denz, C., Alpmann, C., Banzer, P., Bauer, T., Karimi, E., Marrucci, L., Padgett, M., Ritsch-Marte, M., Litchinitser, N.M., Bigelow, N.P., Rosales-Guzmán, C., Belmonte, A., Torres, J.P., Neely, T.W., Baker, M., Gordon, R., Stilgoe, A.B., Romero, J., White, A.G., Fickler, R., Willner, A.E., Xie, G., McMorran, B., Weiner, A.M.: Roadmap on structured light. J. Opt **19**(1), 013001 (2017)
20. Bozinovic, N., Yue, Y., Ren, Y., Tur, M., Kristensen, P., Huang, H., Willner, A.E., Ramachandran, S.: Terabit-scale orbital angular momentum mode division multiplexing in fibers. Science **340**(6140), 1545–1548 (2013)
21. Toyoda, K., Takahashi, F., Takizawa, S., Tokizane, Y., Miyamoto, K., Morita, R., Omatsu, T.: Transfer of light helicity to nanostructures. Phys. Rev. Lett **110**(14), 143603 (2013)
22. Kozawa, Y., Matsunaga, D., Sato, S.: Superresolution imaging via superoscillation focusing of a radially polarized beam. Optica **5**(2), 86 (2018)
23. Deng W., Chen X., Zhao F., Dong J.: Transverse angular momentum in topological photonic crystals. J. Optics **20**, 014006 (2018)
24. Bao, J., Fu, Z., Pramanik, T., Mao, J., Chi, Y., Cao, Y., Zhai, C., Mao, Y., Dai, T., Chen, X., Jia, X., Zhao, L., Zheng, Y., Tang, B., Li, Z., Luo, J., Wang, W., Yang, Y., Peng, Y., Liu, D., Dai, D., He, Q., Muthali, A.L., Oxenløwe, L.K., Vigliar, C., Paesani, S., Hou, H., Santagati, R., Silverstone, J.W., Laing, A., Thompson, M.G., O'Brien, J.L., Ding, Y., Gong, Q., Wang, J.: Very-large-scale integrated quantum graph photonics. Nat. Photonics **17**(7), 573–581 (2023)
25. Elshaari, A.W., Pernice, W., Srinivasan, K., Benson, O., Zwiller, V.: Hybrid integrated quantum photonic circuits. Nat. Photonics

14(5), 285–298 (2020)
26. Zelaya, K., Honari-Latifpour, M., Mandal, K.K., Friedman, J., Madamopoulos, N., Miri, M.A.: On-chip unitary generation of arbitrary complex spatial photonic states. Optica **12**(9), 1492 (2025)
27. Yablonovitch, E.: Photonic band-gap structures. J. Opt. Soc. Am. B **10**(2), 283 (1993)
28. Yablonovitch, E.: Inhibited spontaneous emission in solid-state physics and electronics. Phys. Rev. Lett **58**(20), 2059–2062 (1987)
29. John, S.: Strong localization of photons in certain disordered dielectric superlattices. Phys. Rev. Lett **58**(23), 2486–2489 (1987)
30. Wang, Y., Wang, H.X., Liang, L., Zhu, W., Fan, L., Lin, Z.K., Li, F., Zhang, X., Luan, P.G., Poo, Y., Jiang, J.H., Guo, G.Y.: Hybrid topological photonic crystals. Nat. Commun **14**(1), 4457 (2023)
31. Chen, Y., He, X.T., Cheng, Y.J., Qiu, H.Y., Feng, L.T., Zhang, M., Dai, D.X., Guo, G.C., Dong, J.W., Ren, X.F.: Topologically protected valley-dependent quantum photonic circuits. Phys. Rev. Lett **126**(23), 230503 (2021)
32. He, X.T., Liang, E.T., Yuan, J.J., Qiu, H.Y., Chen, X.D., Zhao, F.L., Dong, J.W.: A silicon-on-insulator slab for topological valley transport. Nat. Commun **10**(1), 872 (2019)
33. Shalaev, M.I., Walasik, W., Tsukernik, A., Xu, Y., Litchinitser, N.M.: Robust topologically protected transport in photonic crystals at telecommunication wavelengths. Nat. Nanotechnol **14**(1), 31–34 (2019)
34. Gao, F., Xue, H., Yang, Z., Lai, K., Yu, Y., Lin, X., Chong, Y., Shvets, G., Zhang, B.: Topologically protected refraction of robust kink states in valley photonic crystals. Nat. Phys **14**(2), 140–144 (2018)
35. Dong, J.W., Chen, X.D., Zhu, H., Wang, Y., Zhang, X.: Valley photonic crystals for control of spin and topology. Nat. Mater **16**(3), 298–302 (2017)
36. Lalau-Keraly, C.M., Bhargava, S., Miller, O.D., Yablonovitch, E.: Adjoint shape optimization applied to electromagnetic design. Opt. Express **21**(18), 21693–21701 (2013)
37. Lu, J., Vučković, J.: Nanophotonic computational design. Opt. Express **21**(11), 13351–13367 (2013)
38. Yang, K.Y., Shirpurkar, C., White, A.D., Zang, J., Chang, L., Ashtiani, F., Guidry, M.A., Lukin, D.M., Pericherla, S.V., Yang, J., Kwon, H., Lu, J., Ahn, G.H., Van Gasse, K., Jin, Y., Yu, S.P., Briles, T.C., Stone, J.R., Carlson, D.R., Song, H., Zou, K., Zhou, H., Pang, K., Hao, H., Trask, L., Li, M., Netherton, A., Rechtman, L., Stone, J.S., Skarda, J.L., Su, L., Vercruysse, D., MacLean, J.W., Aghaeimeibodi, S., Li, M.J., Miller, D.A.B., Marom, D.M., Willner, A.E., Bowers, J.E., Papp, S.B., Delfyett, P.J., Aflatouni, F., Vučković, J.: Multi-dimensional data transmission using inverse-designed silicon photonics and microcombs. Nat. Commun **13**(1), 7862 (2022)
39. Piggott, A.Y., Lu, J., Lagoudakis, K.G., Petykiewicz, J., Babinec, T.M., Vučković, J.: Inverse design and demonstration of a compact and broadband on-chip wavelength demultiplexer. Nat. Photonics **9**(6), 374–377 (2015)
40. Su, L., Piggott, A.Y., Sapra, N.V., Petykiewicz, J., Vučković, J.: Inverse design and demonstration of a compact on-chip narrowband three-channel wavelength demultiplexer. ACS Photonics **5**(2), 301–305 (2018)
41. Mohammadi Estakhri, N., Edwards, B., Engheta, N.: Inverse-designed metastructures that solve equations. Science **363**(6433), 1333–1338 (2019)
42. Camacho, M., Edwards, B., Engheta, N.: A single inverse-designed photonic structure that performs parallel computing. Nat. Commun **12**(1), 1466 (2021)
43. Sapra, N.V., Yang, K.Y., Vercruysse, D., Leedle, K.J., Black, D.S., England, R.J., Su, L., Trivedi, R., Miao, Y., Solgaard, O., Byer, R.L., Vučkovicć, J.: On-chip integrated laser-driven particle accelerator. Science **367**(6473), 79–83 (2020)
44. White, A.D., Su, L., Shahar, D.I., Yang, K.Y., Ahn, G.H., Skarda, J.L., Ramachandran, S., Vučković, J.: Inverse design of optical vortex beam emitters. ACS Photonics **10**(4), 803–807 (2023)
45. Goodman, J.W.: Introduction to Fourier Optics. 3rd ed. Roberts & Company Publishers (2005)
46. Nape, I., Singh, K., Klug, A., Buono, W., Rosales-Guzman, C., McWilliam, A., Franke-Arnold, S., Kritzinger, A., Forbes, P., Dudley, A., Forbes, A.: Revealing the invariance of vectorial structured light in complex media. Nat. Photonics **16**(7), 538–546 (2022)
47. Lin, X., Wei, M., Lei, K., Yang, S., Ma, H., Zhong, C., Luo, Y., Li, D., Li, J., Lin, C., Zhang, W., Dai, S., Hu, X., Li, L., Li, E., Lin, H.: Compact mid-infrared chalcogenide glass photonic devices based on robust-inverse design. Laser Photonics Rev **17**(2), 2200445 (2023)
48. Wei, M., Lin, X., Xu, K., Wu, Y., Wang, C., Wang, Z., Lei, K., Bao, K., Li, J., Li, L., Li, E., Lin, H.: Inverse design of compact nonvolatile reconfigurable silicon photonic devices with phase-change materials. Nanophotonics **13**(12), 2183–2192 (2024)

Zijia Wang received the B.S. degree in Computer Science and Technology from Hefei University of Technology. She is currently pursuing the M.S. degree in Electronic Information at Zhejiang University. Her research interests focus on the inverse design of nanophotonic devices using intelligent algorithms, including machine learning and topology optimization.

Kunhao Lei received the B.S. degree in Materials Science and Engineering from Wuhan University of Technology. He is currently pursuing the Ph.D. degree in Electronic Information at Zhejiang University. His research focuses on chalcogenide integrated photonic devices, on-chip photonic memristors, and CMOS back-end-compatible polysilicon modulators.

Shenglong Yang received the B.S. degree from Sichuan University, Chengdu, China, in 2023. He is currently pursuing the Ph.D. degree with the College of Optical Science and Engineering, Zhejiang University, Hangzhou, China. His research interests focus on integrated photonics, with a particular emphasis on acousto-optic coupling in nanophotonic structures.

Mengxue Qi received the B.S. degree from Sun Yat-sen University. She is currently a research assistant with the Sulfur-based Optoelectronics Laboratory, Zhejiang University. Her research interests include chalcogenide optoelectronic materials and integrated photonic devices.

Jieren Song received the B.E. degree in Electronic Science and Technology from Zhejiang University in 2020. He is currently working toward the M.E. degree in Electronic Science and Technology with the College of Information Science and Electronic Engineering, Zhejiang University, Hangzhou, China. His research is focused on the design and fabrication of metasurfaces and their applications in computational imaging.

Yuting Ye received the B.S. degree from Zhejiang Sci-Tech University, and the M.S. and Ph.D. degrees from Zhejiang University. She is currently a Postdoctoral Researcher with Westlake University. Her research interests focus on flexible photodetectors and multidimensional flexible image sensors, with applications in wearable optoelectronics and imaging systems.

Hui Ma received the B.S. degree in Microelectronics Science and Engineering from Central South University. He obtained the Ph.D. degree in Electronic Science and Technology from Zhejiang University. He is currently a postdoctoral researcher at Nanyang Technological University (NTU). His research interests focus on mid-infrared waveguide-integrated photodetectors.

Yiting Yun received the B.S. degree from Xidian University and the M.S. degree in Electronic Science and Technology from Zhejiang University. She is currently pursuing the M.S. degree in Electronic Science and Technology at Zhejiang University. Her research focuses on chalcogenide integrated optoelectronic materials and devices.

Qiwei Zhan received the B.S. degree from the University of Science and Technology of China, Hefei, China, in 2013, the M.S. degree in Civil and Environmental Engineering from Duke University, Durham, NC, USA, in 2016, and the Ph.D. degree in Electrical and Computer Engineering from Duke University (U.S. News: No. 8 in the U.S.), in 2019. From June 2019 to August 2020, he was a Peter O'Donnell, Jr. Postdoctoral Fellow in Oden Institute for Computational Engineering and Sciences (CWUR: No. 1 in the World for CSE, with 8/47 full-time faculty as Academicians), at University of Texas, Austin. Since September 2020, he has been with the College of Information Science and Electronic Engineering at Zhejiang University as a Professor and Ph.D. Supervisor. His research interests include multiphysics modeling, computational mechanical waves, computational electromagnetics, uncertainty quantification, effective medium theory, inverse problems, biomedical imaging, and scientific machine learning.

Da Li (Member, IEEE) received the B.S. and Ph.D. degrees in Electrical Engineering from Zhejiang University, Hangzhou, China, in 2014 and 2019, respectively. From 2019 to 2021, he was with Science and Technology on Antenna and Microwave Laboratory, Nanjing, China, as a Research Fellow. He is currently an Assistant Professor with Zhejiang University. His research interests include machine learning, antennas, metasurfaces, and electromagnetic compatibility. Dr. Li has authored or coauthored more than 50 refereed papers and served as Reviewers for 6 technical journals and TPC Members of 3 IEEE conferences. He was also a recipient of the Outstanding Young Scientist Award at 2022 Asia-Pacific International Symposium on Electromagnetic Compatibility.

Shixun Dai received the Ph.D. degree in Materials from the Shanghai Institute of Optics and Fine Mechanics, Chinese Academy of Sciences, Shanghai, China, in 2003. He joined Ningbo University, Ningbo, China, in 2005 and founded the Laboratory of Infrared Materials and Devices. He is currently the Vice President of Ningbo University and the Director of the Laboratory of Infrared Materials and Devices. He has authored or coauthored more than 200 publications and 100 patents. His research focuses on specical glass fibers and their photonic devices.

Baile Zhang is currently a Professor of Physics in the School of Physical and Mathematical Sciences, Nanyang Technological University (NTU). Before he joined NTU in 2011, he was a postdoctoral associate at Singapore-MIT Alliance for Research and Technology Centre in Singapore. He received the Ph.D. degree in 2009 from MIT, following the B.S. degree in 2003 and M.S. degree in 2006 from Tsinghua University in Beijing, all majored in Electrical Engineering. His current research interests include waves in complex media, metamaterials, and photonic/acoustic crystals. He was awarded the 2012 MIT Technology Review TR35 Global Young Innovators Award, the 2014 Young Scientist Award of Singapore National Academy of Science, and the 2016 IPS World Scientific (Physics Research) Medal and Prize. In 2020, with Prof. Nikolay Zheludev and Prof. Chong Yidong, he was awarded Singapore's President's Science Award.

Xiaoyong Hu received the B.S. degree (1995) and the M.S. degree (2001) from Hebei University, and the Ph.D. degree (2004) from the Institute of Physics, Chinese Academy of Sciences. From 2004 to 2006, he was a Postdoctoral Researcher with the School of Physics, Peking University. Since 2006, he has been with the Institute of Modern Optics, School of Physics, Peking University, where he is currently a Professor and Ph.D. Supervisor. His research interests include mesoscopic optics and micro-/nano-photonics. Prof. Hu is a recipient of the Rao Yutai Prize in Basic Optics (Second Prize, 2007), the MOE New Century Excellent Talents Program (2010), the Wang Xuan Young Scholar Award (2010), and the National Natural Science Award of China (Second Prize, 2011; second contributor). He was awarded the National Science Fund for Distinguished Young Scholars (2012), selected as a Changjiang Distinguished Professor (2015), and recognized by China's Innovation Talent Promotion Plan (2016) and the National "Ten Thousand Talents Program" (2017). He served as Topical Editor for *Optics Letters* (2012–2018), and is/has been an Editorial Board Member/Editor for *Scientific Reports* (2015–present), *Frontiers of Optoelectronics* (2019–present), and *Frontiers in Physics.*

Lan Li obtained the B.S. degree from University of Science and Technology of China (2010) and Ph.D. degree from University of Delaware (2016), both in Materials Science and Engineering. Since then she has been a postdoctoral associate at Massachusetts Institute of Technology for three years. Dr. Li joined Westlake University as an assistant professor in February 2019. Her research interest focuses on nanophotonic materials and devices, infrared optical glass materials, integrated flexible photonic device fabrication, characterization, and applications.

Erping Li (foreign academician of the Chinese Academy of Engineering (CAE)) was the Founding Dean of the Joint Institute of Zhejiang University–University of Illinois at Urbana-Champaign, Zhejiang University, Hangzhou, China, in 2016. Since 1993, he has been a Research Fellow, an Associate Professor, a Professor, a Principal Scientist, and the Senior Director of Singapore Research Institute and University, Singapore. He is currently a Qiushi-Distinguished Professor with the Department of Information Science and Electronic Engineering, Zhejiang University. His research interests include electrical modeling and design of micro/nano scale integrated circuits and 3D electronic package integration. Dr. Li is a fellow of IEEE, USA Electromagnetics Academy and Singapore Academy of Engineering. He was a recipient of the IEEE EMC Technical Achievement Award in 2006, Singapore IES Prestigious Engineering Achievement Award and the Changjiang Chair Professorship Award in 2007, the 2015 IEEE Richard Stoddard Award on EMC, the 2021 IEEE EMC Laurence G.Cumming Award, and Zhejiang Natural Science 1st Class Award. He has been the general chair and the technical chair of many international conferences. He was the President of the 2006 International Zurich Symposium on EMC, the Founding General Chair of Asia–Pacific EMC Symposium, and the General Chair of the 2008, 2012, 2016, 2018, 2022 APEMC, and 2010 IEEE Symposium on Electrical Design for Advanced Packaging Systems. He has been invited to give 120 invited talks and plenary speeches at various international conferences and forums.

Hongtao Lin received the B.S. degree from University of Science and Technology of China in 2010, and the Ph.D. degree from the University of Delaware in 2015. From 2015 to 2018, he was a Postdoctoral Associate with Massachusetts Institute of Technology. Since 2018, he has been with the College of Information Science and Electronic Engineering, Zhejiang University, where he is currently a Tenured Associate Professor ("Hundred Talents Program" Researcher), Ph.D. Supervisor, and Deputy Head of the Department of Electronic Engineering. He is a recipient of China's National High-Level Talent Program for Young Professionals and a Zhejiang Provincial Distinguished Expert. Dr. Lin's research interests include silicon photonics and heterogeneous photonic integration, with a focus on chalcogenide (sulfur-based) optoelectronics for integrated optical-field manipulation and photonic computing, mid-infrared integrated optoelectronic sensing and communications, and infrared metasurfaces for wavefront control and imaging systems. He has authored or coauthored over 100 papers in leading journals, including *Nature Photonics*, *Light: Science & Applications*, *Optica*, and *Nature Communications*, with more than 7,400 citations and an H-index of 41. His group's work on heterogeneous photonic integration was selected as "Optics in 2018" by Optics & Photonics News, and "On-Chip Infrared Optoelectronic Logic-Gate Intelligent Chip" was recognized as one of China's Top Ten Optical Advances in 2023 (Applied Research). He also received a nomination award for "Three-Year Outstanding Achievements in Silicon Photonics" for the backend-of-line integration of nonvolatile silicon photonic devices.

Authors and Affiliations

Zijia Wang[1*] · Kunhao Lei[1*] · Shenglong Yang[1*] · Mengxue Qi[1] · Jieren Song[1] · Yuting Ye[2] · Hui Ma[1] · Yiting Yun[1] · Qiwei Zhan[1] · Da Li[1] · Shixun Dai[3] · Baile Zhang[4] · Xiaoyong Hu[5] · Lan Li[2] · Erping Li (✉)[1] · Hongtao Lin (✉)[1,6]

✉ Erping Li
liep@zju.edu.cn

Hongtao Lin
hometown@zju.edu.cn

[1] State Key Laboratory of Brain-Machine Intelligence, Key Laboratory of Micro-Nano Electronics and Smart System of Zhejiang Province, College of Information Science and Electronic Engi-

neering, Zhejiang University, Hangzhou 310027, China

[2] Key Laboratory of 3D Micro/Nano Fabrication and Characterization of Zhejiang Province, School of Engineering, Westlake University, Hangzhou 310024, China

[3] Laboratory of Infrared Materials and Devices, Ningbo University, Ningbo 315211, China

[4] Division of Physics and Applied Physics, School of Physical and Mathematical Sciences, Nanyang Technological University, Singapore 637371, Singapore

[5] State Key Laboratory for Mesoscopic Physics, Frontiers Science Center for Nano-optoelectronics, School of Physics, Peking University, Beijing 100871, China

[6] MOE Frontier Science Center for Brain Science & Brain-Machine Integration, Zhejiang University, Hangzhou 310027, China